SAMIR: SPARSITY AMPLIFIED BEAMFORMING FOR HIGH-RESOLUTION ULTRASOUND IMAGING

Amol G Mahurkar[*,1], *Praveenkumar Pokala*[*,1], *Chetan Singh Thakur*[2], *Chandra Sekhar Seelamantula*[1]

[1]Department of Electrical Engineering, [2]Department of Electronic Systems Engineering
Indian Institute of Science, Bangalore-12, India
amolgmahurkar@gmail.com, {praveenkumar, csthakur}@iisc.ac.in, chandra.sekhar@ieee.org

ABSTRACT

In ultrasound imaging, one typically employs delay-and-sum (DAS) beamformers for image reconstruction. An apodization window is typically used to suppress the side-lobes of an array beam pattern. The application of an apodization window to suppress the side-lobes typically widens the main-lobe width. We consider a statistical beamformer and present two variants. The signal of interest is modeled as a Laplacian-distributed random variable and additive interference components as Gaussian distributed. The resultant LASSO formulation is known to suffer from underestimation of large signal amplitudes due to the ℓ_1 norm regularization. In the first variant, we reformulate the LASSO problem with a minimax-concave penalty (called Sparsity AMplified (SAM)) to contain the bias, thereby enhancing the beamformed image. A closed-form pointwise estimator is obtained for the optimization problem. In the second variant, we propose Sparsity AMplified Iteratively-Reweighted (SAMIR) beamforming algorithm, which leverages the properties of an apodization function. In SAMIR beamforming, we jointly optimize the cost over the signal-of-interest and the extrinsic apodization weights. This beamformer results in high-resolution ultrasound images, especially in the lateral direction. The proposed methods are compared with the standard DAS and a recently proposed statistically-modeled beamformer, iMAP, for a different number of plane-wave insonifications.

Index Terms— ultrasound imaging, beamforming algorithm, apodization function, non-convex penalty, sparsity amplification.

1. INTRODUCTION

In ultrasound B-mode imaging, typically, a transmission, of either a focused or an unfocused acoustic beam (through a linear array transducer), is followed by recording of received signals. In order to generate the B-mode image, the received signals are time-aligned by appropriate delays, defined by the array geometry and the angle of transmission and reception. The delays attempt to isolate the on-axis echoes originating from a particular point. In conventional delay-and-sum (DAS) beamforming, the aligned signals are averaged to obtain the beamformed image. Due to a finite aperture T, the off-axis echoes are not entirely suppressed. As a result, the DAS beam pattern is characterized by a main-lobe and several side lobes, which correspond to the Fourier transform of a rectangular aperture. To counter these effects, an apodization window, independent of the received signals, is applied to reduce the main-lobe width and suppress the side lobes significantly.

* Equal contribution. This work was supported by the MHRD - IMPacting Research INnovation and Technology (IMPRINT) project of the Government of India (IMPR-6000).

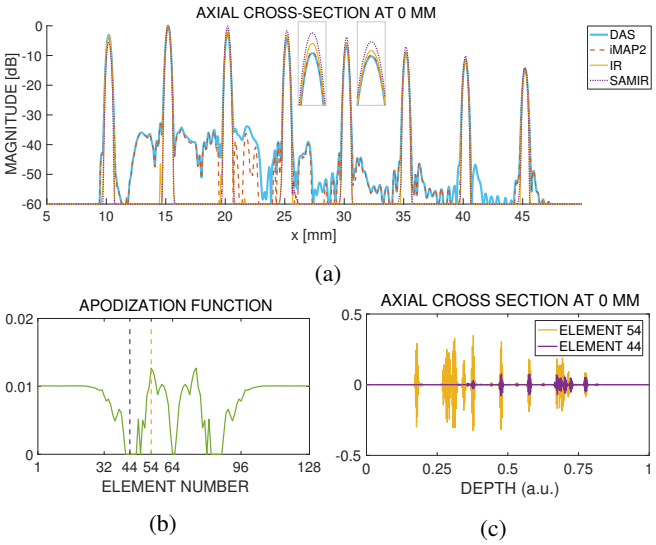

Fig. 1: [color online] (a) Plot highlights the amplification of the signal with SAMIR compared with IR beamforming algorithm. It can be seen that both beamformers surpasses the conventional DAS, and the recently proposed iMAP BF algorithm. Optimal apodization function in (b) highlights weight of two elements with (c) their corresponding aperture signals.

The inherent trade-off between the main-lobe width and the side-lobe level, due to the uncertainty principle, limits the performance of a beamformer. A sharper main-lobe corresponds to a finer resolution, and lower side-lobe levels correspond to a higher contrast in the image domain. A signal-dependent reweighting of the received signals is considered in Capon's Minimum Variance (MV) [1] beamformer such that it maintains unity gain in the desired direction while minimizing the energy received from the other directions. This method requires estimation and inversion of a covariance matrix for every pixel in the image. Due to its sensitivity to estimation errors, additional strategies such as spatial smoothing and diagonal loading are incorporated to improve robustness [2–5]. Lorenz and Boyd generalized Capon's method (MV) by accounting for the uncertainty in the array response and/or the imprecise knowledge of the angle of arrival [6].

In literature, several signal-dependent reweighing techniques such as Wiener beamforming [7], coherence factor (CF) [8], scaled Wiener postfilter (ScW) [9] have been proposed to improve the image contrast. The coherence factor assumes coherence of the signal originating at the focal point over aperture elements in contrast to

the interference [10–13]. The coherence factor is thus defined as the ratio of coherent to incoherent sums across the detected signals. Despite the advantages, the resultant images of CF may suffer from reduced image brightness, especially in low SNR conditions. Nilsen and Holm in [9] critically analyzed the coherence factor beamforming in the context of Wiener beamforming. The scaled Wiener postfilter combines the contrast improvement of CF and robustness of Wiener filtering.

Recently, Eldar et al. statistically modeled [14] the signal of interest and the additive interference components in the received time-aligned signals. They considered the underlying desired signal and interference components to be uncorrelated Gaussian random variables. The proposed beamformer, iMAP, is shown to be superior in terms of contrast-to-noise ratio than other state-of-the-art algorithms reported in the literature.

In this paper, we model the signal of interest and additive interference components in the received time-aligned signals as random variables. In particular, the signal of interest is assumed to follow a Laplacian p.d.f. and the interference a normal p.d.f., which requires us to solve a special instance of the LASSO [15] problem and has a pointwise estimator with a free parameter. It is known in the literature that an ℓ_1 penalty in the LASSO formulation underestimates large signal amplitudes [16]. We rectify the bias by reformulating the LASSO problem with a non-convex penalty [17, 18], and provide a pointwise estimator with two free parameters. We further extend these formulations to optimize over the extrinsic apodization weights given typical constraints on the apodization functions such as tapering, symmetry and non-negative – this approach requires an iterative solver. An illustration of optimal weights from SAMIR technique is shown in Figure 1b.

Recently, a class of non-convex penalties has been proposed by Selesnick that generalizes an ℓ_1 norm while maintaining the convexity of the overall least-squares cost [16]. The proposed minimax-concave (MC) penalty is the difference between an ℓ_1 norm and a parameterized Huber function. It bridges the gap between the ℓ_1 norm and an ℓ_p norm ($0 < p < 1$). The advantage of MC penalty over the ℓ_1 norm is that it provides a more accurate estimation of the large amplitudes and promotes higher level of sparsity.

2. SIGNAL MODEL

Consider a beamforming framework for an M-element linear array transducer. We transmit either a plane wave or a focused beam (depending on the imaging mode) into the medium, and record the echoes received at all M elements. The received signal at the m^{th} element, $\hat{y}_m(t)$, is then delayed by applying appropriate delays $\tau_m(t;\theta)$ (depending on the array geometry) focusing in the direction θ to get aperture data $y_m(t;\theta)$. The time-aligned signal $y_m(t)$ has an underlying signal $x(t)$ which is of interest to us. Considering that the beamforming process is identical for every θ, we simplify the notation by dropping θ in further discussion. Therefore, for a particular angle θ, the aperture data can be decomposed as

$$y_m(t) = x(t) + n_m(t), \tag{1}$$

where $n_m(t)$ is due to off-axis reflections, multi-path interference and channel noise. In vector form, at time t, equation (1) can be expressed as

$$\mathbf{y}_t = x_t\, \mathbf{1}_M + \mathbf{n}_t, \tag{2}$$

where $\mathbf{1}_M$ is an M-length column vector of all ones, and $\mathbf{y}_t, \mathbf{n}_t \in \mathbb{R}^M$. We also define $\mathbf{x} = [x_1, \cdots, x_N] \in \mathbb{R}^N$ and $\mathbf{Y} = [\mathbf{y}_1, \cdots, \mathbf{y}_N]^{\mathrm{T}} \in \mathbb{R}^{N\times M}$ for N time samples.

The goal is to estimate x_t from the aperture data $\mathbf{y}_t$ for a time t. We assume that entries in $\mathbf{n}_t$ are Gaussian distributed, $\mathbf{n}_t \sim \mathcal{N}(\mathbf{0}, \sigma_n^2\mathbf{I})$, where $\mathbf{I}$ is the $M \times M$ identity matrix and σ_n^2 is the noise variance.

If the signal of interest x_t is deterministic, then the ML estimate is given by

$$\begin{aligned} x_{\text{ML},t} &= \arg\, \max_x p(\mathbf{y}_t; x), \\ &= \frac{1}{M}\mathbf{1}_M^{\mathrm{T}}\mathbf{y}_t = \sum_{m=1}^{M} w_m\, y_{m,t}, \end{aligned} \tag{3}$$

where $w_m = 1/M$, $\forall m \in [\![1, M]\!]$. Thus, the Gaussian noise model and deterministic signal of interest result in the classic delay-and-sum (DAS) beamforming solution.

3. SPARSITY AMPLIFIED BEAMFORMING

We assume that the signal of interest is a random variable with a Laplacian p.d.f. (uncorrelated with noise), that is, $x_t \sim \mathcal{L}(0, \beta_s)$, where β_s is the signal scale. Consider the maximum a posteriori (MAP) estimate of x_t:

$$\begin{aligned} x_{\text{MAP},t} &= \arg\, \max_x p(\mathbf{y}_t|x)p(x), \\ &= \arg\, \max_x \sum_{m=1}^{M} \log p(y_{m,t}|x)p(x), \\ &= \arg\, \min_x \sum_{m=1}^{M} \frac{(y_{m,t}-x)^2}{2\sigma_n^2} + \frac{|x|}{\beta_s}, \\ &= \arg\, \min_x \sum_{m=1}^{M} \frac{1}{2}(y_{m,t}-x)^2 + \lambda\,|x|\,, \end{aligned} \tag{4}$$

where $\lambda = \sigma_n^2/\beta_s$. We now impose an apodization function w_m as follows

$$x_{\text{MAP},t} = \arg\, \min_x \sum_{m=1}^{M} \frac{1}{2}(y_{m,t}w_m - x)^2 + \lambda\,|x|\,. \tag{5}$$

Here, we consider w_m to be constant and summing up to 1 for all $m \in [\![1, M]\!]$. Rewriting (5) in vector form using matrix-vector notations results in

$$\mathbf{x}_{\text{MAP}} = \arg\, \min_{\mathbf{x}} \underbrace{\frac{1}{2}\|\mathbf{Y}\mathbf{w} - \mathbf{x}\|_2^2 + \lambda\|\mathbf{x}\|_1}_{J(\mathbf{x})}, \tag{6}$$

which is a standard problem of LASSO [15]. We note here that the ℓ_1-penalty is separable in x. The minimizer of $J(\mathbf{x})$ is given by a simple formula:

$$\mathbf{x}_{\text{MAP}} = \text{ST}_\lambda\left(\mathbf{Y}\mathbf{w}\right), \tag{7}$$

where ST_λ is the element-wise soft-thresholding operator [19] defined as

$$\text{ST}_\kappa(z) = \max\left(0, |z| - \kappa\right)\, \text{sign}(z).$$

Following the time separability in (5), we thus have a pointwise MAP estimate $\mathbf{x}_{\text{MAP}}$ for every time t. The problem of LASSO is known to suffer from underestimation of large signal amplitudes due to the ℓ_1 penalty (and its corresponding proximal operator) [16]. The underestimation of signal amplitudes is evident in Figure 4,

comparing ST with DAS and iMAP estimates. Next, we reformulate the LASSO problem to contain and address the underestimation issue.

Consider the following optimization problem consisting of a quasiconvex minimax-concave penalty (MC), $\phi_\mu(\mathbf{x})$:

$$\mathbf{x}_{\text{SAM}} = \arg\min_{\mathbf{x}} \underbrace{\frac{1}{2}\|\mathbf{Y}\mathbf{w} - \mathbf{x}\|_2^2 + \lambda\,\phi_\mu(\mathbf{x})}_{G(\mathbf{x})}, \tag{8}$$

where

$$\phi_\mu(x) = \begin{cases} |x| - \dfrac{x^2}{2\mu}, & |x| \le \mu, \\ \dfrac{\mu}{2}, & |x| \ge \mu, \end{cases} \tag{9}$$

Since the penalty $\phi_\mu(\mathbf{x})$ is a separable in x, it can be applied element-wise. Even though the penalty $\phi_\mu(\mathbf{x})$ is non-convex in general, the overall cost function $G(\mathbf{x})$ is convex for $\mu > \lambda$ [16]. The minimizer is given by

$$\mathbf{x}_{\text{SAM}} = \mathcal{F}_{\lambda,\mu}\left(\mathbf{Y}\mathbf{w}\right), \tag{10}$$

where $\mathcal{F}_{\lambda,\mu}$ is the element-wise firm-thresholding operator

$$\mathcal{F}_{\lambda,\mu}(z) = \begin{cases} 0, & |z| \le \lambda, \\ \dfrac{\mu\left(|z| - \lambda\right)}{\mu - \lambda}\text{sign}(z), & \lambda \le |z| \le \mu, \\ z, & |z| \ge \mu. \end{cases} \tag{11}$$

The SAM estimate in (10) rectifies the underestimation of large signal amplitudes as seen in Figure 4. The SAM estimate in large amplitude regions is now comparable to the DAS and iMAP2 solutions while attenuating the spurious amplitudes (as seen in DAS and iMAP2). Also, this reformulation provides pointwise estimates as the MAP estimate.

4. SPARSITY AMPLIFIED ITERATIVELY-REWEIGHTED (SAMIR) BEAMFORMING

In the previous section, we chose the apodization weights to be constant, normalized to unity. Typically, an apodization window is tapering, symmetric, and non-negative. Some examples include the rectangular window, Hamming window, and Hann window. We now optimize over apodization weights, $\mathbf{w}$, the ST-associated cost function $J(\mathbf{w})$.

To determine the optimal apodization weights $\mathbf{w}$ satisfying the properties listed above, one must solve the following optimization problem:

$$\begin{aligned} \{\mathbf{x}_{\text{IR}}, \tilde{\mathbf{w}}_{\text{IR}}\} &= \arg\min_{\mathbf{x},\tilde{\mathbf{w}}} J(\mathbf{x}, \mathbf{S}\tilde{\mathbf{w}}), \\ \text{subject to} \quad & \mathbf{1}_M^{\text{T}}\mathbf{w} = 1, \\ & \mathbf{w} \succcurlyeq \mathbf{0}, \\ & \mathbf{w} = \mathbf{S}\tilde{\mathbf{w}}, \end{aligned} \tag{12}$$

where $\mathbf{S} = [\mathbf{I},\, \mathbf{P}]^{\text{T}} \in \{0,1\}^{M\times(M/2)}$ for imposing symmetry on $\mathbf{w}$, with $\mathbf{I}$ being the identity matrix, and $\mathbf{P}$ being the permutation matrix, and $\succcurlyeq$ denotes componentwise inequality.

The constraints are incorporated using an augmented Lagrangian $\boldsymbol{L}_J$:

$$\boldsymbol{L}_J(\mathbf{x}, \mathbf{w}, \xi) = J(\mathbf{x}, \mathbf{w}) + \langle\, \xi\,, \mathbf{1}_M^{\text{T}}\mathbf{w} - 1\,\rangle + \frac{\rho}{2}\|\mathbf{1}_M^{\text{T}}\mathbf{w} - 1\|_2^2, \tag{13}$$

Algorithm 1 Sparsity AMplified Iteratively-Reweighted (SAMIR) Beamformer.

Require: $\mathbf{Y}$ - Aperture data
Initialize: $\lambda, \mu, \xi_0, \rho, \epsilon$
$\mathbf{x}_0 \leftarrow \mathbf{0}$
$\mathbf{w}_0 \leftarrow \frac{1}{M}\mathbf{1}_M$
$i \leftarrow 0$
repeat
  Update $\mathbf{x}_i$:
  $\mathbf{x}_{i+1} \leftarrow \mathcal{F}_{\lambda,\mu}\left(\mathbf{Y}\mathbf{w}_i\right)$
  Update $\mathbf{w}_i$:
  $\tilde{\mathbf{w}}_{i+1} \leftarrow \left[\left(\mathbf{Y}^{\text{T}}\mathbf{Y} + \rho\mathbf{1}_M\mathbf{1}_M^{\text{T}}\right)\mathbf{S}\right]^{\dagger}$
  $\left[\mathbf{Y}\mathbf{x}_{i+1} - (\xi_i - \rho)\,\mathbf{1}_M\right]$
  $\tilde{\mathbf{w}}_{i+1} \leftarrow \text{ReLU}(\tilde{\mathbf{w}}_{i+1})$
  $\mathbf{w}_{i+1} \leftarrow \mathbf{S}\tilde{\mathbf{w}}_{i+1}$
  Dual ascent:
  $\xi_{i+1} \leftarrow \xi_i + \rho(\mathbf{1}_M^{\text{T}}\mathbf{w}_{i+1} - 1)$
  $i \leftarrow i + 1$
until convergence: $\|\mathbf{x}_i - \mathbf{x}_{i-1}\|_2 / \|\mathbf{x}_{i-1}\|_2 < \epsilon$
$\mathbf{x}_{\text{SAMIR}} \leftarrow \mathbf{x}_i$
$\mathbf{w}_{\text{SAMIR}} \leftarrow \mathbf{w}_i$

where ξ is the Lagrange multiplier. The solution to (12) is found at the saddle point of the augmented Lagrangian $\boldsymbol{L}_J(\mathbf{x}, \mathbf{w}, \xi)$, and is solved using the augmented Lagrangian method (ALM) [20].

As seen before, the ℓ_1-penalty-based formulation suffers from underestimation of large signal amplitudes, so will an estimate $\mathbf{x}_{\text{IR}}$ with optimal weights $\mathbf{w}_{\text{IR}}$ in previous section. We now optimize over the apodization weights, $\mathbf{w}$, the SAM-associated cost $G(\mathbf{x})$ in (8). In particular, we solve the following optimization problem:

$$\begin{aligned} \{\mathbf{x}_{\text{SAMIR}}, \tilde{\mathbf{w}}_{\text{SAMIR}}\} &= \arg\min_{\mathbf{x},\tilde{\mathbf{w}}} G(\mathbf{x}, \mathbf{S}\tilde{\mathbf{w}}), \\ \text{subject to} \quad & \mathbf{1}_M^{\text{T}}\mathbf{w} = 1, \\ & \mathbf{w} \succcurlyeq \mathbf{0}, \\ & \mathbf{w} = \mathbf{S}\tilde{\mathbf{w}}. \end{aligned} \tag{14}$$

The solution to (14) is found by solving the sub-optimization routines over the variables $(\mathbf{x}, \mathbf{w}, \xi)$, for the augmented Lagrangian $\boldsymbol{L}_G(\mathbf{x}, \mathbf{w}, \xi)$, using an ALM as described in Algorithm 1. We use Rectified Linear Units (ReLU) to impose the non-negativity constraint. To solve (12), we replace $\mathcal{F}_{\lambda,\mu}$ with the ST_λ operator.

5. SIMULATION RESULTS

In this work, we would like to highlight the amplitude enhancement and the high-resolution capability of the SAMIR beamforming algorithm. To demonstrate, we use pre-beamformed data from the PICMUS dataset [21]. The raw data is acquired using the Field-II ultrasound simulation software with a 128-element transducer of center frequency 5.208 MHz, sampled at 20.832 MHz.

The raw data is acquired for different number of plane wave (PW) insonifications. To test the high-resolution capability of the SAMIR beamforming (BF) algorithm, we use a point-reflector phantom from the PICMUS dataset. In addition, we simulate the directivity pattern of an array with lower side lobes by applying a Hann window with an f-number of 1.75 on reception. As a consequence, the contrast of an image is improved at the expense of a wider main-lobe, thereby affect-

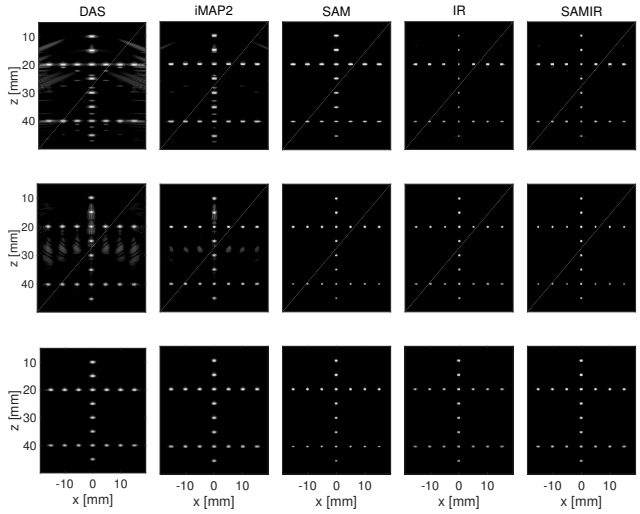

Fig. 2: Simulation results for 1 plane wave (1st row), 11 plane wave (2nd row), 75 plane wave (3rd row) insonifications; Dynamic range of all images is 60 dB.

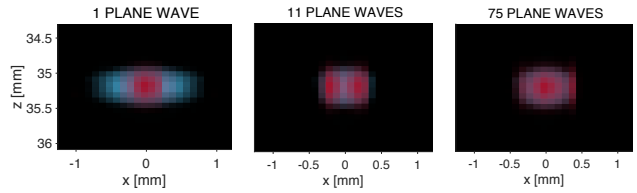

Fig. 3: [color online] Point reflector comparison between SAM (blue) and SAMIR (red) BF algorithm; Dynamic range of all images is 60 dB.

ing its resolution in the image domain. In the case of a Hann window, its main-lobe width is given by $8\pi/T$, where T is the window size, whereas the rectangular window has a width of $4\pi/T$. In contrast, the peak side-lobe level for Hann window is -31.5 dB, whereas a rectangular window has -13.3 dB.

In Figure 4, we first highlight the rectification of the underestimation of signal amplitudes using the proposed reformulation of the LASSO problem in (8). The pointwise estimate $\mathbf{x}_{\text{SAM}}$ restores the signal strength compared with the ST estimate $\mathbf{x}_{\text{MAP}}$, and is comparable to DAS and iMAP2 estimates. Here, iMAP2 refers to two iterations of the iMAP beamforming algorithm. Furthermore, the SAM estimate prevents spurious magnitude regions as seen around the axial location of 15 and 25 mm (of DAS and iMAP) in Figure 4.

We further present the optimal apodization function $\mathbf{w}_{\text{SAMIR}}$ in Figure 1b, highlighting two weights and their corresponding aperture signals in Figure 1c. The optimal apodization functions $\mathbf{w}_{\text{IR}}$ and $\mathbf{w}_{\text{SAMIR}}$ lead to high-resolution images as evident from the measured lateral resolutions of IR and SAMIR BF algorithm in Table 1 as compared to SAM and other beamforming techniques. The axial and lateral resolutions are evaluated as an average over all point reflectors within the image. The resolution in each direction is computed as the full width at half maximum (FWHM) of the Point Spread Function (PSF). The axial resolution of the proposed techniques (SAM and SAMIR) is comparable to that of others.

Table 1: A Comparison of the Measured Axial and Lateral Resolution (in mm) for Various Beamforming Algorithms.

Measure	**1 plane wave**		**11 plane waves**		**75 plane waves**	
	Axial res.	*Lat. res.*	*Axial res.*	*Lat. res.*	*Axial res.*	*Lat. res.*
DAS	0.40	1.17	0.40	0.60	0.40	0.63
iMAP2	0.39	1.08	0.40	0.59	0.40	0.63
SAM	0.36	1.10	0.36	0.54	0.36	0.57
IR	0.37	0.59	0.38	0.47	0.40	0.59
SAMIR	0.37	**0.45**	0.38	**0.40**	0.40	**0.58**

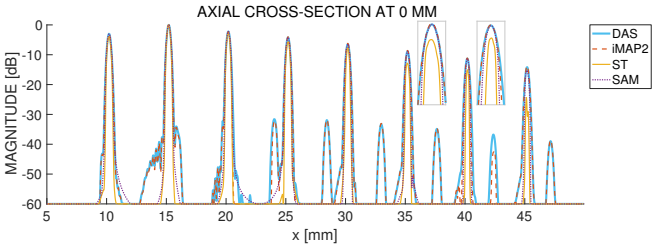

Fig. 4: [color online] Plot highlights the underestimation of signal amplitudes with ℓ_1-based ST (eq. 7) and its rectification with MC penalty-based SAM (eq. 10) beamforming algorithm.

The simulation results with different number of plane wave insonifications are shown in Figure 2. The point reflectors estimated using IR and SAMIR BF algorithm have a similar resolution, except for the underestimation of amplitudes in IR. The SAM recovers the amplitudes but lacks the high-resolution capability of SAMIR as highlighted in Figure 3.

In conclusion, the joint optimization (in IR and SAMIR beamforming) over the signal of interest, and the extrinsic apodization weights lead to high-resolution imaging, whereas the sparsity amplification assists SAMIR enhance the signal amplitudes as well. The proposed beamforming algorithm, SAMIR, is compared to the classic DAS and the recently proposed iMAP beamformer in Figure 1a.

6. CONCLUSION

In this paper, we considered a statistical beamformer with Laplacian distributed signal prior, and a Gaussian interference. The resulting formulation (i.e., LASSO) is known to suffer from the amplitude underestimation. To ameliorate the bias, we proposed a formulation based on the non-convex minimax-concave penalty. We demonstrated its efficacy in rectifying the amplitude bias, and suppression of the spurious amplitudes resulting in sharp point-reflectors of the phantom. We further incorporate the properties of the apodization function into a constrainted optimization problem to get high-resolution images. The joint optimization, with respect to the signal of interest and the apodization weights, resulted in finely resolved images, especially in lateral direction. We integrated the high-resolution formulation with the sparsity-enhancing minimax-concave penalty resulting in the enhanced high-resolution ultrasound images. The proposed beamformer, SAMIR, shows superior lateral resolution and amplitude-enhanced image compared to the classic DAS and a recently proposed statistical beamformer called iMAP. We note that further extensive analysis is needed in choosing the regularization parameters and its impact on the overall image reconstruction. Also, validation on other phantoms is required for facilitating its use in real-world applications.

7. REFERENCES

[1] J. Capon, "High-resolution frequency-wavenumber spectrum analysis," *Proceedings of the IEEE*, vol. 57, no. 8, pp. 1408–1418, 1969.

[2] A. Austeng, C. C. Nilsen, A. C. Jensen, S. P. Näsholm, and S. Holm, "Coherent plane-wave compounding and minimum variance beamforming," in *Proc. 2011 IEEE Ultrasonics Symposium (IUS)*, pp. 2448–2451.

[3] N. Q. Nguyen and R. W. Prager, "Minimum variance beamformers for coherent plane-wave compounding," in *Medical Imaging 2017: Ultrasonic Imaging and Tomography*. International Society for Optics and Photonics, 2017, vol. 10139, p. 1013912.

[4] F. Vignon and M. R. Burcher, "Capon beamforming in medical ultrasound imaging with focused beams," *IEEE Transactions on Ultrasonics, Ferroelectrics, and Frequency Control*, vol. 55, no. 3, pp. 619–628, 2008.

[5] M. Sasso and C. C.-Bacrie, "Medical ultrasound imaging using the fully adaptive beamformer," in *Proc. IEEE Intl. Conf. on Acoustics, Speech, and Signal Processing*. IEEE, 2005, vol. 2, pp. ii–489.

[6] R. Lorenz and S. Boyd, "Robust minimum variance beamforming," *IEEE Transactions on Signal Processing*, vol. 53, no. 5, pp. 1684–1696, 2005.

[7] H. L. Van Trees, *Detection, Estimation, and Modulation Theory, Part I: Detection, Estimation, and Linear Modulation Theory*, John Wiley & Sons, 2004.

[8] K. Hollman, K. Rigby, and M. O'donnell, "Coherence factor of speckle from a multi-row probe," in *Proc. 1999 IEEE Ultrasonics Symposium, 1999*. IEEE, 1999, vol. 2, pp. 1257–1260.

[9] C. Nilsen and S. Holm, "Wiener beamforming and the coherence factor in ultrasound imaging," *IEEE Transactions on Ultrasonics, Ferroelectrics, and Frequency Control*, vol. 57, no. 6, pp. 1329–1346, 2010.

[10] S.-L. Wang, C.-H. Chang, H.-C. Yang, Y.-H. Chou, and P.-C. Li, "Performance evaluation of coherence-based adaptive imaging using clinical breast data," *IEEE Transactions on Ultrasonics, Ferroelectrics, and Frequency Control*, vol. 54, no. 8, pp. 1669–1679, 2007.

[11] B. M. Asl and A. Mahloojifar, "Minimum variance beamforming combined with adaptive coherence weighting applied to medical ultrasound imaging," *IEEE Transactions on Ultrasonics, Ferroelectrics, and Frequency Control*, vol. 56, no. 9, pp. 1923–1931, 2009.

[12] S.-L. Wang and P.-C. Li, "MVDR-based coherence weighting for high-frame-rate adaptive imaging," *IEEE Transactions on Ultrasonics, Ferroelectrics, and Frequency Control*, vol. 56, no. 10, pp. 2097–2110, 2009.

[13] M. Xu, Y. Chen, M. Ding, and Y. Ming, "Adaptive minimum variance beamforming combined with phase coherence imaging for ultrasound imaging," in *Medical Imaging 2012: Ultrasonic Imaging, Tomography, and Therapy*. International Society for Optics and Photonics, 2012, vol. 8320, p. 83200E.

[14] T. Chernyakova, D. Cohen, M. Shoham, and Y. Eldar, "iMAP beamforming for high quality high frame rate imaging," June 2018, arXiv:1806.03526 [Online]. Available: https://arxiv.org/abs/1806.03526.

[15] M. Elad, *Sparse and Redundant Representations: From Theory to Applications in Signal and Image Processing*, Springer Publishing Company, Incorporated, 1st edition, 2010.

[16] I. Selesnick, "Sparse Regularization via Convex Analysis," *IEEE Transactions on Signal Processing*, vol. 65, no. 17, pp. 4481–4494, 2017.

[17] I. Selesnick, "Sparsity Amplified," in *Proc. 2017 IEEE International Conference on Acoustics, Speech and Signal Processing (ICASSP)*. IEEE, pp. 4356–4360.

[18] C.-H. Zhang et al., "Nearly unbiased variable selection under minimax concave penalty," *The Annals of Statistics*, vol. 38, no. 2, pp. 894–942, 2010.

[19] I. Daubechies, M. I. Defrise, and C. De Mol, "An iterative thresholding algorithm for linear inverse problems with a sparsity constraint," *Communications on Pure and Applied Mathematics*, vol. 57, no. 11, pp. 1413–1457, 2004.

[20] D. P. Bertsekas, *Nonlinear programming*, Athena Scientific Belmont, 1999.

[21] H. Liebgott, A. Rodriguez-Molares, F. Cervenansky, J. Jensen, and O. Bernard, "Plane-wave imaging challenge in medical ultrasound," in *Ultrasonics Symposium (IUS), 2016 IEEE International*. IEEE, 2016, pp. 1–4.